Journal of Geophysical Research: Space Physics

RESEARCH ARTICLE
10.1029/2018JA025751

Variations of Field Line Eigenfrequencies With Ring Current Intensity

J. K. Sandhu[1], T. K. Yeoman[2], and I. J. Rae[1]

[1]Department of Space and Climate Physics, Mullard Space Science Laboratory, University College London, Dorking, UK, [2]Department of Physics and Astronomy, University of Leicester, Leicester, UK

Key Points:
- Time-of-flight estimates considerably improve our understanding of global variations in eigenfrequencies with geomagnetic activity
- Magnetic field changes are the dominant factor in eigenfrequency variations with ring current strength
- Variations in the eigenfrequency with geomagnetic activity provide insight into storm time energization of the radiation belts

Supporting Information:
- Supporting Information S1

Correspondence to:
J. K. Sandhu,
j.sandhu@ucl.ac.uk

Citation:
Sandhu, J. K., Yeoman, T. K., & Rae, I. J. (2018). Variations of field line eigenfrequencies with ring current intensity. *Journal of Geophysical Research: Space Physics*, *123*, 9325–9339. https://doi.org/10.1029/2018JA025751

Received 4 JUN 2018
Accepted 31 OCT 2018
Accepted article online 5 NOV 2018
Published online 21 NOV 2018

Abstract We present results from the closed magnetosphere ($5.9 \leq L < 9.5$ over all magnetic local times) to demonstrate and assess the variations in field line eigenfrequency with geomagnetic activity. Using the time-of-flight technique with realistic magnetic field and mass density models, the spatial distributions of field line eigenfrequencies are determined for a range of different geomagnetic activity levels, as defined by the Dst index. The results indicate that during geomagnetically active conditions, the eigenfrequency of a given field line is generally decreased compared to quiet times, in addition to variations in local asymmetries. By comparing the dependence to changes in the magnetic field and mass density distribution, it is established that the inflation and weakening of the geomagnetic field outweighs decreased plasma mass density and is the sole contributor to decreased eigenfrequencies with increased geomagnetic activity. We highlight the importance of considering the magnetic field, mass density, and average ion mass contributions when using observed eigenfrequencies to probe magnetospheric conditions. Furthermore, the estimates significantly improve upon existing time-of-flight results, through a consideration of mass density changes with geomagnetic activity. We also provide estimates of eigenfrequencies for a comparatively extended spatial region than available from prior direct observations of field line resonances. The results have clear implications for furthering our understanding of how wave energy propagates throughout the magnetosphere during geomagnetic storms.

Plain Language Summary The Earth's magnetic field experiences resonant oscillations of individual magnetic field lines at discrete frequencies, known as eigenfrequencies, which play an important role in transporting energy throughout the Earth's space environment. The frequencies of these oscillations can be highly variable, and a key factor in this variability is the strength of the geomagnetic ring current. In this study, we employ realistic models describing the magnetic field configuration and the spatial distribution of the plasma mass density, which also account for variations with ring current intensity. This allows us to estimate how the eigenfrequencies vary for different levels of ring current strength. We explore changes in the magnitude as well as the spatial distribution. A key result is an observed decrease in the magnitude of the eigenfrequency with increased ring current strength. This result has important implications for understanding how energy can access regions closer to the Earth and consequently act to significantly energize the plasma.

1. Introduction

Shear Alfvén waves are defined as transverse oscillations of magnetic field lines occurring in a plasma. In the terrestrial magnetosphere, for the case when the wavelength of an Alfvén wave is comparable to the length of a closed geomagnetic field line, a standing Alfvén wave can occur. The standing Alfvén waves, commonly termed FLRs (field line resonances), occur at resonant frequencies, or eigenfrequencies, that are controlled by the magnetic field and plasma properties (Dungey, 1954a; 1954b; Southwood, 1974). FLRs and their eigenfrequencies play a key role in magnetospheric physics through the transfer of energy and momentum throughout the magnetospheric system (e.g., Elkington et al., 1999; Goertz & Smith, 1989; Hartinger et al., 2011; Rae et al., 2007).

In the terrestrial magnetosphere, the magnetic field and plasma properties are highly variable, both in L shell, MLT (magnetic local time), and for different levels of geomagnetic activity. Consequently, the eigenfrequencies of field lines vary too. For example, work by Sandhu, Yeoman, et al. (2018) explored field line

eigenfrequencies for typical magnetospheric conditions and demonstrated strong spatial dependences, in terms of both *L* shell and local time. It is known that the magnetic field and plasma experience dramatic changes with geomagnetic activity, particularly during geomagnetic storms (Akasofu & Chapman, 1961; Akasofu et al., 1963; Chapman, 1918; Chapman & Bartels, 1940; Gonzalez et al., 1994). Therefore, it is important to understand how the eigenfrequencies of field lines respond to different levels of geomagnetic activity. The response of the eigenfrequencies and properties of FLRs has important implications for understanding how wave energy propagates throughout the magnetosphere during storm and substorm processes. In particular, it has been demonstrated that FLRs play a key role in the energization of the radiation belts during geomagnetic storms (Baker, Pulkkinen, Li, Kanekal, Ogilvie, et al., 1998; Baker, Pulkkinen, Li, Kanekal, Blake, et al., 1998; Green & Kivelson, 2001; Mathie & Mann, 2000; Nakamura et al., 2002; O'Brien & Moldwin, 2003; Rostoker et al., 1998), and establishing how the spatial distribution of eigenfrequencies varies with geomagnetic activity will provide further insight into the energization interaction.

Previous work has provided an insight into the average variations of field line eigenfrequencies with geomagnetic activity, although there is limited analysis of the general trends. Takahashi et al. (2002) explored the dependence of observed toroidal FLRs on Kp index for field lines with *L* values spanning from 6 to 10. The results showed clear dependences on the level of geomagnetic activity. However, the spatial coverage of the analysis was restricted to cover only the dawn sector (04–06 MLT). Here we aim to assess changes in the field line eigenfrequencies with geomagnetic activity with increased spatial coverage and provide a more global understanding.

2. Time-of-Flight Calculations

In order to assess changes in field line eigenfrequency, we employ the time-of-flight technique, which allows us to estimate the eigenfrequency of a given field line under defined conditions (Sandhu, Yeoman, et al., 2018; Warner & Orr, 1979; Wild et al., 2005). The time-of-flight method is now briefly summarized here. By considering the propagation of an Alfvén wave along a closed geomagnetic field line, the resonant eigenfrequency of the field line is determined by the field line length and the Alfvén speed. The Alfvén speed, v_A, is defined as

$$v_A = \frac{B}{\sqrt{\mu_0 \rho}} \tag{1}$$

where B is the magnetic field strength, ρ is the plasma mass density, and $\mu_0 (= 4\pi \times 10^{-7})$ H m^{-1} is the permeability constant. Equation (1) shows that the Alfvén velocity is dependent on the magnetic field strength and the plasma mass density.

Considering the FLR simply as a standing Alfvén wave on a closed geomagnetic field line, the time-of-flight technique involves calculating the time taken for an Alfvén perturbation to traverse the full field line length. The inverse of this time provides the frequency of the field line oscillation. Therefore, the eigenfrequency, f, can be expressed as

$$\frac{1}{f} = 2 \int \frac{ds}{v_A} \tag{2}$$

where the integral is over the full field line length, s. The time-of-flight technique requires an assumption of the magnetic field line length, s, as well as how the field strength, B, and plasma mass density, ρ, vary along the field line. Although this technique is relatively simplistic, it has been established to provide reasonably valid estimates of the field line eigenfrequencies in the region considered here (Sandhu, Yeoman, et al., 2018), as well as good agreement compared to the Singer et al. (1981) approach (Wild et al., 2005). Wild et al. (2005) demonstrated that equatorward of approximately 70° magnetic latitude, the numerically calculated eigenfrequency using the (Singer et al., 1981) estimation is approximately 75% of the equivalent time-of-flight calculated eigenfrequency.

2.1. Mass Density Model

As shown by equations (2) and (1), the time-of-flight techniques require an assumed magnetic field and distribution of total plasma mass density along a given field line in order to estimate the eigenfrequency. Previous work employing the time-of-flight technique to estimate field line eigenfrequencies have incorporated increasingly realistic magnetic field configurations, although relatively simplistic mass density models were assumed (Lee & Lysak, 1990; Warner & Orr, 1979; Wild et al., 2005). In contrast, a study conducted by Sandhu, Yeoman, et al. (2018) explored using the time-of-flight technique with both a realistic magnetic field

model and a realistic mass density model. Specifically, the T96 magnetic field model (Tsyganenko, 1995; 1996) and an empirically derived mass density model based on Cluster observations (Sandhu et al., 2016a; 2016b) were assumed. The choice of mass density model accounts for several features neglected by previous mass density models, such as the inclusion of an equatorial enhancement in mass density and the inclusion of the ion composition contribution, and therefore represents a significant improvement compared to previous models (Sandhu et al., 2016a, 2016b). Furthermore, the model is based on a relatively substantial data set of observations spanning several years (2001–2012), with good spatial coverage over all local times between $5.9 \leq L < 9.5$.

This model was extended by Sandhu et al. (2017) to include dependences of the plasma mass density distribution on geomagnetic activity. Sandhu et al. (2017) parameterized the spatial mass density distribution with Dst index, considering Dst index values ranging from −100 to 10 nT. The Dst index describes the global magnetic field perturbation measured by a range of ground magnetometer stations, whose locations map to the ring current region (Iyemori, 1990; Sugiura & Kamei, 1991; Sugiura & Poros, 1964). Consequently, it is commonly used as a proxy for the ring current intensity, where large negative perturbations correspond to an enhanced ring current (Chapman, 1918; Dessler & Parker, 1959; Sckopke, 1966). Therefore, the model presented by Sandhu et al. (2017) provides a description of how the spatial distribution of total plasma mass density varies with the ring current strength. Analysis of the mass density dependence on the level of geomagnetic activity showed that the number density of magnetospheric plasma was observed to decrease with increasing activity, which was expected to result from the increased magnetospheric convection during active times. In contrast, the average ion mass of the plasma was observed to increase, as increased heavy ion outflows at high latitudes are convected into the inner magnetosphere. During active conditions, the decreased number density dominates over the competing average ion mass. This results in a general decrease in the total plasma mass density for $5.9 \leq L < 9.5$. Overall, the model showed that the total plasma mass density distribution possesses significant dependences on geomagnetic activity.

In this study, we utilize Dst index dependent mass density and magnetic field models in the time-of-flight technique to explore how field line eigenfrequencies change with the level of geomagnetic activity. The T96 magnetic field model is used, which is a semiempirical model parameterized by the solar wind dynamic pressure, P_{dyn}, the IMF (interplanetary magnetic field) B_y and B_z components, and the Dst index. The time-of-flight analysis provides insight into how the large-scale spatial distributions of field line eigenfrequencies respond to enhanced ring current conditions and how they are determined through the combination of the magnetic field and mass density contributions.

3. Estimates of Field Line Eigenfrequencies

The time-of-flight technique is used to estimate the field line eigenfrequencies for a range of field lines at different levels of Dst index using equation (2). The T96 magnetic field model and the Sandhu et al. (2017) mass density model are assumed. Figure 1 shows the estimated frequencies for a range of field lines covering all MLTs and $5.9 \leq L < 9.5$. Note that this spatial region is constrained by the L-MLT coverage of the Sandhu et al. (2017) mass density model, rather than the magnetic field model. Each row corresponds to a different value of Dst index, where values from −100 nT (active conditions) to 0 nT (quiet conditions) have been considered. The magnetic field model and plasma mass density model were parameterized by the Dst index. The remaining parameters required for the T96 magnetic field model (P_{dyn}, IMF B_y, and IMF B_z) were set to their averages for each value of the Dst index, over a time period spanning 2001–2012. This time period is consistent with the Sandhu et al. (2017) mass density model. Table 1 shows the average parameter values for each Dst index value considered here. As expected, Table 1 demonstrates that during active geomagnetic conditions the solar wind typically exhibits higher solar wind dynamic pressure, larger magnitude of magnetic field components, and stronger southward component of the IMF (e.g., Dungey, 1961; Snyder et al., 1963; Wilcox et al., 1967; Zhang et al., 2006). The values shown in Table 1 are used in the T96 magnetic field model for the corresponding Dst index value in the following time-of-flight calculations.

The left panels of Figure 1 show the eigenfrequencies plotted at the field lines' position in the magnetic equatorial plane, and the right panels show the eigenfrequencies plotted at the field lines' ionospheric footprint in the Northern Hemisphere. Note that the footprint latitude coverage shown in the right panels of Figure 1 varies with Dst index due to the mapping of field lines, as the inner magnetospheric field lines expand during times of enhanced ring current.

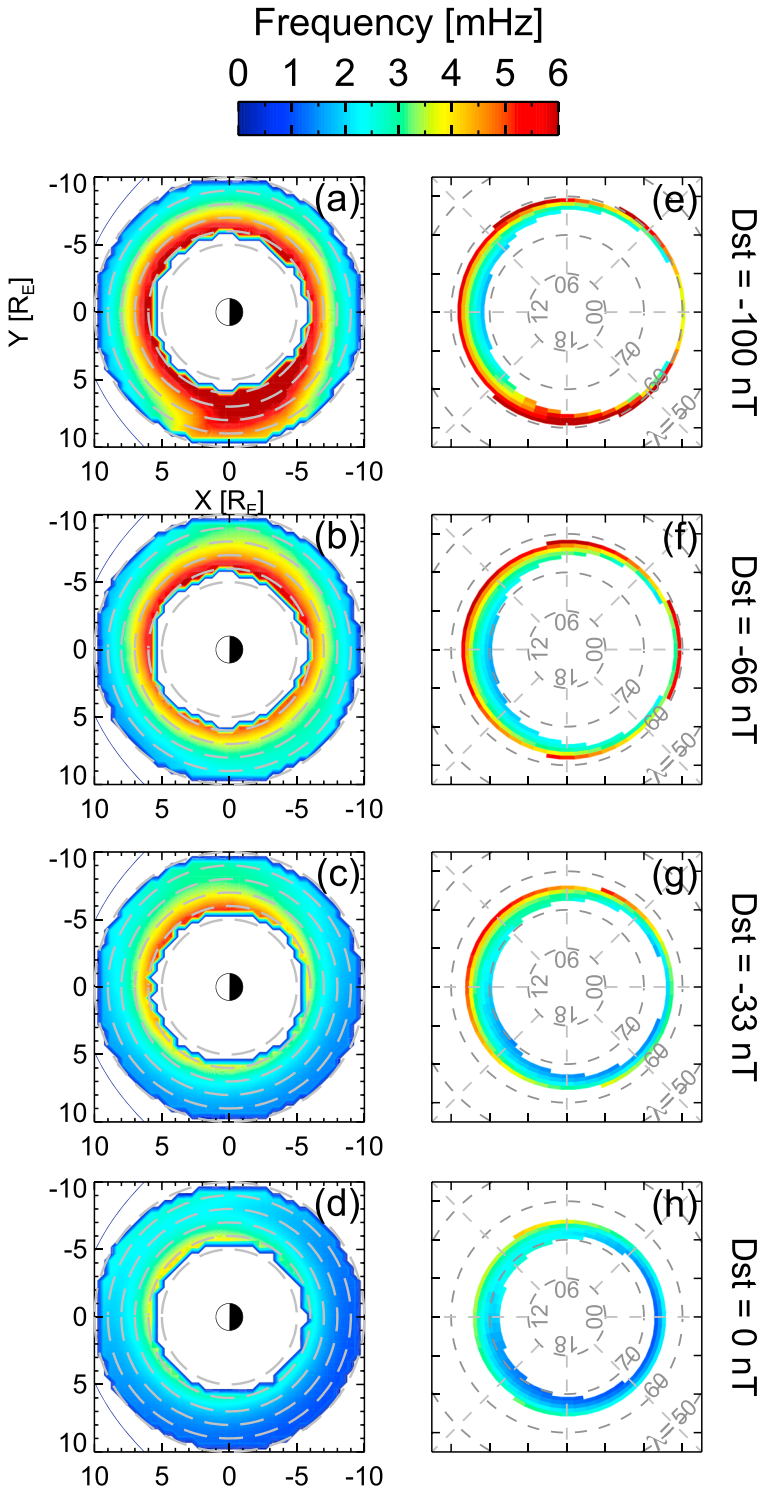

Figure 1. Field line eigenfrequency calculated using the time-of-flight approximation. (a–d) The eigenfrequencies mapped to the field lines' position in the magnetic equatorial plane. (e–h) The eigenfrequencies mapped to the altitude-adjusted corrected geomagnetic latitude and magnetic local time of the field line footprints in the Northern Hemisphere. Each row corresponds to frequencies calculated for different values of the Dst index, as labeled on the right of the panels.

Table 1
The Average Solar Wind and IMF Parameters for Each Value of Dst Index During 2001–2012

Dst index (nT)	P_{dyn} (nPa)	B_y (nT)	B_z (nT)
0	1.8	−0.2	0.6
−33	2.3	−0.1	−1.0
−66	3.3	0.3	−2.4
−100	3.3	1.3	−5.1

Note. IMF = interplanetary magnetic field.

Figure 1 shows significant changes in the spatial distribution with Dst index, both in terms of magnitude and local time asymmetries. Examining variations in eigenfrequency at the equatorial plane, Figures 1a–1d shows an apparent increase in eigenfrequency with increasingly negative Dst index values. However, comparing the changes to the corresponding distributions mapped to the field line footprint positions (Figures 1e–1h, we can determine that the field line configuration has changed significantly. Field lines with L values spanning from 5.9 to 9.5 map to lower-latitude regions with increasingly disturbed conditions. This expected feature is due to an inflation of the magnetic field lines by the enhanced ring current (Cahill, 1970; Ganushkina et al., 2010; Parker & Stewart, 1967; Tsyganenko & Mukai, 2003), such that the radial distance at which a field line crosses the magnetic equatorial plane moves outwards away from the Earth. Therefore, the L value of a given field line changes with Dst index. In order to ensure we compare changes in eigenfrequency with Dst index for the same field line, Figures 1e– 1h show the changes for field lines at their footprint location. We can observe changes in the eigenfrequencies, although due to the changes in where the field lines map to it is difficult to compare the eigenfrequencies for a given footprint latitude. Variations in the MLT asymmetries are apparent from Figure 1. The MLT asymmetry is such that during quiet conditions (Dst index = 0 nT) the peak frequencies are observed in the morning sector. In contrast, moving toward disturbed conditions, the MLT location of peak frequencies shifts westward to the premidnight sector at Dst index value of −100 nT.

Figure 1 demonstrates that the mapping of field lines between the magnetic equatorial plane and the ionospheric footprint plays a significant role in shaping how the spatial distributions of eigenfrequency vary with geomagnetic activity. Whereas field lines mapped to the magnetic equatorial plane appear to exhibit clear global increases in field line eigenfrequency with increased geomagnetic activity (Figures 1a–1d), the distribution mapped to the ionospheric footprints of the field lines (Figures 1e–1h) show different trends. Furthermore, existing reports and investigations of how eigenfrequencies vary with geomagnetic activity consist of both ground-based and spacecraft observations. In order to examine the estimated eigenfrequencies shown in Figure 1 in the context of the existing observations, we consider the spatial distributions under both mapping regimes separately and compare to the relevant previous work. This approach should account for any complexities that the field line mapping introduces.

3.1. Variations at the Magnetic Equatorial Plane

First, the spatial distributions mapped to the magnetic equatorial plane, as shown in Figures 1a–1d, are assessed. To allow for comparisons of eigenfrequency variations with Dst index more quantitatively, L profiles and MLT profiles are shown in Figures 2 and 3. The colored profiles correspond to the use of the mass density model and the magnetic field model at different values of Dst index, as labeled.

The L profiles of the eigenfrequency are shown in Figure 2 for a range of different Dst index values, and it can be seen that the values increase with increased geomagnetic activity. This is consistent across all MLTs. The magnitude of the increase is most significant at lower L values. For example, Figure 2a shows that at 00 MLT the increase in eigenfrequency between 0 and −100 nT is $\sim$ 4 mHz at $L \sim 5$, compared to an increase of $\sim$ 0.5 mHz at $L \sim 9$. The physical processes that are expected to shape the dependences apparent in the estimated eigenfrequencies will be discussed further in section 4.

Figure 3 shows how the estimated eigenfrequencies vary with MLT in the magnetic equatorial plane, and how the MLT profile changes with Dst index. It can be seen that, for all L values, the MLT profile demonstrates significant dependences on the Dst index. Similarly to Figure 2, a general increase in eigenfrequency with increased geomagnetic activity is observed, most significantly at lower L values (Figure 3a). Figure 3 also indicates that the magnitude of the eigenfrequency change has local time variations. During quiet times (red profiles) the

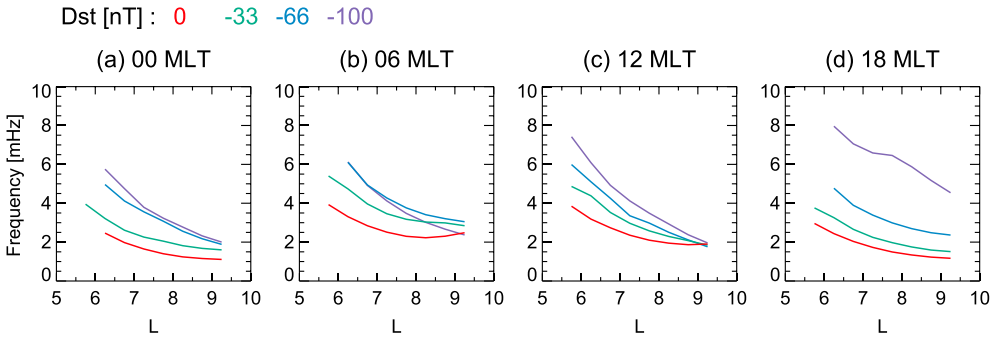

Figure 2. Field line eigenfrequency as a function of *L*. Each color profile shows eigenfrequencies calculated for various Dst index values, where the legend above the panels indicates the color coding of the profiles. Each panel corresponds to field lines at (a–d) different magnetic local times (MLTs), as labeled.

eigenfrequency maximizes in the morning sector. With an increased level of geomagnetic activity, the eigenfrequency exhibits the largest increase in the dusk sector, which acts to shift the MLT asymmetry such that the eigenfrequencies maximize in the evening sector (purple profiles).

3.2. Variations at the Ionosphere

As previously discussed, the large changes in the magnetic field configuration with increasing geomagnetic activity have significant consequences in how the estimated eigenfrequencies are mapped to the ionospheric footprints of the field lines. Consequently, we consider the spatial distributions mapped to the ionosphere independently. Latitudinal and MLT profiles of the eigenfrequency are taken from the distributions shown in Figure 1 and are shown in Figures 4 and 5. The colored profiles correspond to the use of the mass density model at different values of Dst index, as labeled.

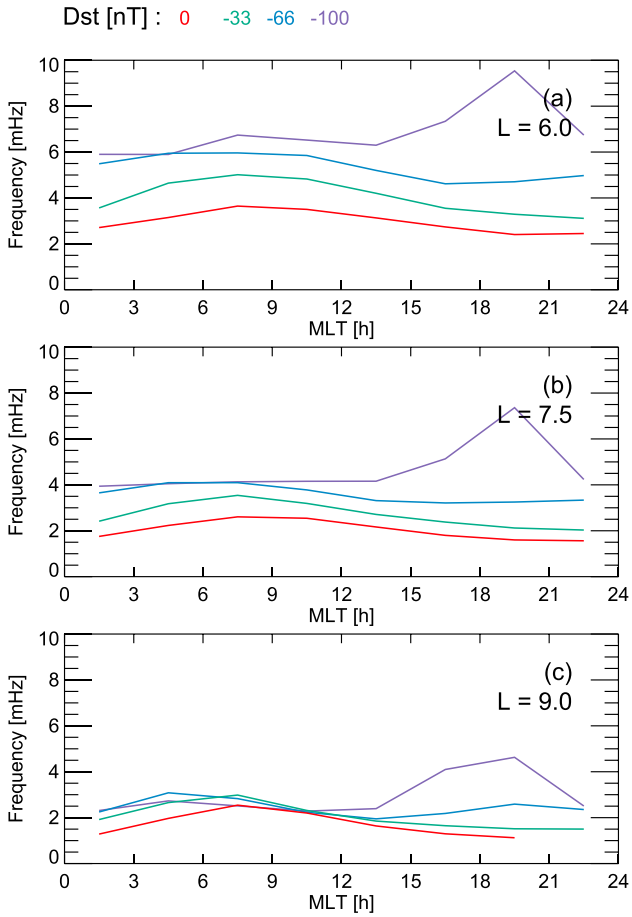

Figure 3. Field line eigenfrequency as a function of magnetic local time (MLT), where each color profile corresponds to calculated eigenfrequencies at different values of the Dst index. The same color coding is used as in Figure 4. Each panel corresponds to field lines with (a–c) different *L* values, as indicated.

In order to examine changes in the eigenfrequency magnitude and latitude dependence with geomagnetic activity, Figure 4 shows the estimated eigenfrequency as a function of footprint latitude, where each color profile corresponds to a different level of Dst index. Furthermore, each panel shows calculated eigenfrequencies for a different MLT meridian. The latitude extent of the profiles shown in Figure 4 is observed to change significantly with Dst index, which is a result of the change in field line configuration and mapping as previously discussed. Given that both the magnetic field and mass density are required for the time-of-flight calculations, only field lines that map to *L* values within 5.9 to 9.5, corresponding to the coverage of the empirical mass density model (Sandhu et al., 2017), can be shown. Regardless, Figure 4 shows that at latitudes where the profiles overlap, particularly apparent in Figure 4c, it is demonstrated that the eigenfrequency of a given field line tends to be reduced for more negative Dst index values. For example, at a footprint latitude of $\sim$ 67° at 12 MLT, the eigenfrequency decreases from $\sim$ 3 mHz at Dst = 0 nT to $\sim$ 2 mHz at Dst = −100 nT. However, the observed magnitudes of the eigenfrequency variations with Dst index are relatively small compared to the latitudinal variations. Furthermore, due to the lack of overlapping coverage at some MLTs (e.g., Figure 4a), it is difficult to assess global changes.

Figure 5 shows the eigenfrequency profiles with MLT, where each color corresponds to a different Dst index value following the same color coding as Figure 4, and each panel shows field lines at a given footprint latitude. It is noted that at higher latitudes (Figure 5c), not all Dst index profiles are shown. This is a consequence of the previously discussed changes in the magnetic field configuration. Field lines at the considered latitude map to *L* values outside of the mass density model coverage ($5.9 \leq L < 9.5$)

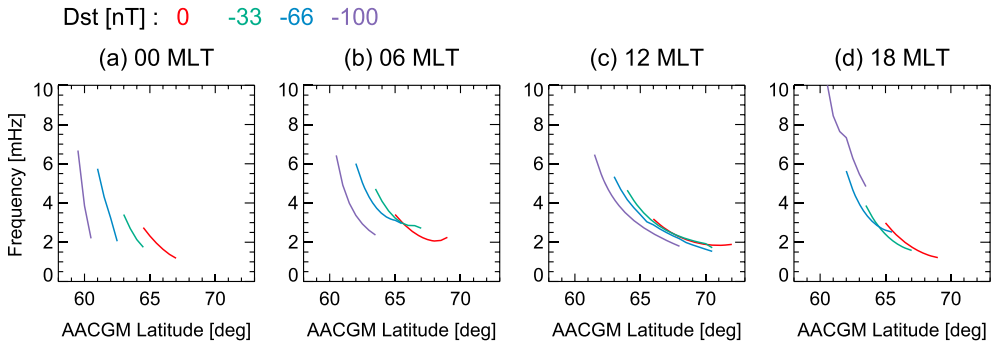

Figure 4. Field line eigenfrequency as a function of altitude-adjusted corrected geomagnetic (AACGM) latitude. Each color profile shows eigenfrequencies calculated for various Dst index values, where the legend above the panels indicates the color coding of the profiles. Each panel corresponds to field lines at (a–d) different magnetic local times (MLTs), as labeled.

and cannot have their eigenfrequency calculated. Figure 5 shows a general decrease in eigenfrequency with increasingly negative Dst index, where this feature was also highlighted from Figures 1e–1h and 4. In addition, a comparison of the panels shown in Figure 5 indicates that the variations in eigenfrequency are larger at lower latitudes. In terms of MLT dependent variations, Figure 5 shows that the decrease in eigenfrequency is most apparent for the morning MLT sectors, whereas in the afternoon the magnitude of the variation is significantly smaller. In the following section we discuss how variations in the magnetic field configuration and mass density distribution with geomagnetic activity may result in the observed changes in field line eigenfrequencies.

To provide an illustrative example of how the eigenfrequency of a given field line can decrease during periods of enhanced geomagnetic activity, we include observations taken from the Canadian Array for Realtime Investigations of Magnetic Activity (CARISMA) ground magnetometer array (Mann et al., 2008). Figure 6 shows results of cross-phase analysis of magnetometer data from the ISLL (Island Lake) and GILL (Gillam) magnetometer stations for (a) 17 March 2013 and (b) 21 March 2013. The B_x component of the ground magnetometer observations are used to compute the cross-phase spectra (Waters et al., 1991). From the cross-phase spectra shown in Figure 6, resonant toroidal oscillations at the field line located at the midpoint of ISLL and GILL ($\sim$ 63°) can be identified as enhancements in the cross-phase value. Figure 6a shows broad enhancements occurring at a frequency of approximately 4 mHz, whereas Figure 6b shows a stable enhancement at $\sim$ 9 mHz. These correspond to the observed eigenfrequency of the field line. The time period considered in Figure 6a is during the main phase of a geomagnetic storm, known as the St. Patrick's Day 2013 storm, where the Dst index reached −132 nT. Figure 6 is during the subsequent late recovery phase. Therefore, we can see that the field line eigenfrequency is significantly depressed during this geomagnetic disturbance, with the general trend in agreement with the estimates presented here. It is noted that during the main phase of the storm (Figure 6a) the observed eigenfrequency of $\sim$ 4 mHz is in good agreement with the time-of-flight values (purple profile at a latitude of $\sim$ 63° in Figure 4c). However, due to the lack of coverage in our estimates, we cannot assess the magnitude of observed eigenfrequency during the late recovery phase.

4. Discussion

By implementing the time-of-flight technique, utilizing a magnetic field and mass density model with Dst index dependences, the variations of field line eigenfrequencies with geomagnetic activity have been estimated. The changes in eigenfrequency are now assessed to explore how the magnetic field and mass density contributions vary with geomagnetic activity levels, and what physical processes are important for determining field line eigenfrequencies.

As illustrated by the time-of-flight technique, there are two key contributors to determining the eigenfrequency of a given field line: the magnetic field configuration and the plasma mass density distribution. Both are known to vary significantly with the level of geomagnetic activity, but how they combine to decide the eigenfrequency of a given field line has been previously unclear.

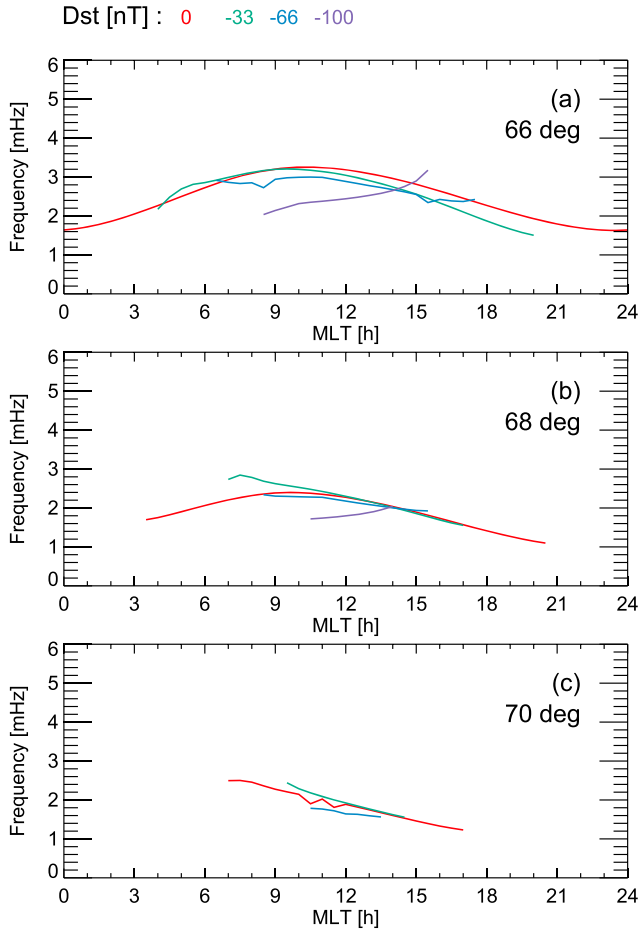

Figure 5. Field line eigenfrequency as a function of magnetic local time (MLT), where each color profile corresponds to calculated eigenfrequencies at different values of the Dst index. The same color coding is used as in Figure 4. Each panel corresponds to field lines at (a–c) different altitude-adjusted corrected geomagnetic latitudes, as indicated.

A study by Wild et al. (2005) revealed how variations in the magnetic field drive changes in the eigenfrequency. Using the time-of-flight technique, with the T96 magnetic field model and a radial power law mass density model (Chappell, 1972; Warner & Orr, 1979), the results showed that with increasingly negative Dst index values the eigenfrequencies are decreased. It is known that during geomagnetically disturbed times, an increase in the ring current energy density results in an increase in the associated magnetic field perturbation. As this perturbation opposes the background geomagnetic field, it acts the expand and weaken the inner magnetosphere (Cahill, 1966, 1970; Ganushkina et al., 2010; Parker & Stewart, 1967; Tsyganenko & Mukai, 2003). Consequently, for a given field line, the field line length is increased for an enhanced ring current, which would act to decrease the field line eigenfrequency (equation (2)). Furthermore, the field strength is reduced, thus decreasing the Alfvén velocity and decreasing the eigenfrequency (equations (1) and (2)). Wild et al. (2005) showed that the overall effect of the magnetic field variations with Dst index results in decreased eigenfrequencies with increasingly negative Dst index, which is due to the weakened and inflated magnetic field.

To expand upon the work presented by Wild et al. (2005), we use a new mass density model that includes dependences on Dst index in the time-of-flight calculations to establish more realistic estimates of the field line eigenfrequencies. In particular, we employ the Sandhu et al. (2017) empirical mass density model. Sandhu et al. (2017) showed that for increasing levels of geomagnetic activity, enhanced O^+-rich outflows are convected from high latitudes to the inner magnetosphere, raising the average ion mass of the plasma. However, enhanced magnetospheric convection of field lines depletes the inner magnetosphere of plasma and dramatically reduces the number density of the plasma. The overall result is a general decrease in the total plasma mass density for active conditions compared to the quiet magnetosphere. Based on the definition of the Alfvén velocity (equation (1)), the change in the mass density would act to increase the eigenfrequency of a given field line, as the Alfvén perturbation can travel more rapidly along the field line length.

Figures 1, 2, and 4 indicate a general decrease in eigenfrequency with L (or equivalently with increasing footprint latitude), consistent for all values of Dst index considered here. This feature is in agreement with multiple previous observations of FLRs and previous time-of-flight analyses (Engebretson et al., 1986; Glassmeier et al., 1984; Liu et al., 2009; Mathie et al., 1999; Obayashi & Jacobs, 1958; Orr & Matthew, 1971; Plaschke et al., 2008; Poulter et al., 1984; Samson et al., 1971; Samson & Rostoker, 1972; Sandhu, Yeoman, et al., 2018; Takahashi et al., 2002, 2004, 2015; Yumoto et al., 1983; Wild et al., 2005). The trend is attributed to decreased magnetic field strength and increased field line length for field lines that extend to increased radial distances, which acts to increase the eigenfrequencies

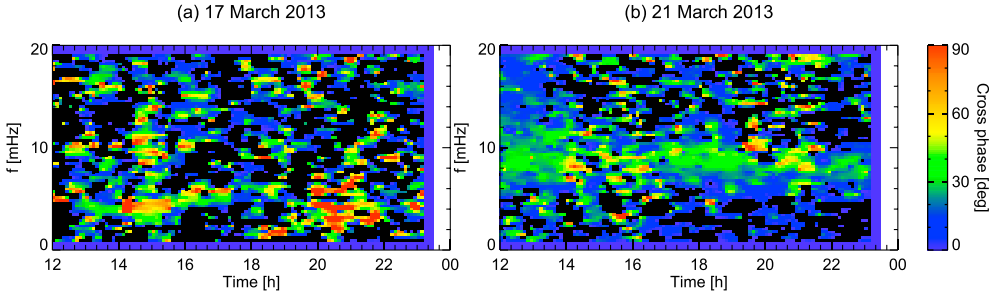

Figure 6. Cross-phase spectra during the (a) main phase and (b) late recovery phase of the St. Patrick's Day 2013 storm from ISLL and GILL B_x ground magnetometer observations.

(equations (1) and (2)). Although the mass density is decreased for field lines extending to increased radial distances, which would correspondingly act to increase the field line eigenfrequencies, the magnetic field variations are dominant and outweigh the mass density contribution (Sandhu, Yeoman, et al., 2018).

The results of the eigenfrequency calculations, shown in Figure 1, demonstrate clear dependences of how the spatial eigenfrequency distribution varies with geomagnetic activity on where the eigenfrequencies are mapped to along the field lines. Consequently, it is appropriate to consider spatial distribution mapped to the magnetic equatorial plane and the ionosphere independently. Figure 2 shows the eigenfrequencies as a function of the field line L value, corresponding to radial variations in the magnetic equatorial plane, and the corresponding local time variations are shown in Figure 3. The results showed that at a given L value, the eigenfrequency increases significantly by up to $\sim$ 5 mHz for Dst values between 0 and −100 nT. The magnitude of the increase in eigenfrequency is largest at low L values in the nightside MLT sector. As previously discussed, the variations in the mass density with geomagnetic activity act to increase the eigenfrequency, whereas the magnetic field variations act to decrease the eigenfrequency. Therefore, the results shown in Figures 2 and 3 suggest that the mass density variations are dominating over the magnetic field variations and act to increase the eigenfrequency. Therefore, this implies that the magnetic field lines at a given L experience relatively small changes in the field line length and the profile of magnetic field strength along the field line with geomagnetic activity (Du et al., 2005). In particular, it is somewhat expected that field lines with a given L value will have similar field line lengths. In terms of the mass density variations, Sandhu et al. (2017) identified that the largest variations in the mass density with geomagnetic activity are observed at low L values in the nightside MLT sector, which is consistent with the eigenfrequency variations and demonstrates how changes in the mass density impart increases in the field line eigenfrequencies.

Existing literature providing spacecraft observations of field line eigenfrequency L profiles for different levels of geomagnetic activity is relatively limited, with inconsistent results. A case study by Engebretson and Cahill (1981) details Explorer 45 observations of resonant pulsations during a geomagnetic storm and observed that the eigenfrequencies in the afternoon MLT sector near $L = 5$ were decreased during the main phase. This contradicts the trends in estimated eigenfrequencies shown in Figures 1–3. A key factor to highlight here is that the time-of-flight calculations are based on the average mass density distributions and the average magnetic field configuration during the time period spanning 2001–2012. Therefore, these estimated eigenfrequencies represent the average trends with geomagnetic activity. On a case by case basis, it is anticipated that there will be variability from the average trends, and so the results of case studies such as Engebretson and Cahill (1981) and Du et al. (2005) differ from the average statistical dependences. In terms of statistical studies, Takahashi et al. (2002) examined Charge Composition Explorer observations in the dawn sector. It was identified that the change in eigenfrequency was L dependent, with both relatively small increases and decreases with Kp index observed. It is noted here that the Kp index and the Dst index contain different contributions from the magnetospheric current systems due to the latitudinal location of the ground magnetometer stations (Bartels et al., 1939; Baumjohann & Treumann, 1996; Sugiura & Kamei, 1991; Sugiura & Poros, 1964; Thomsen, 2004), and as such may incur some differences with the parameterization. In order to allow for a clear and accurate comparison and validation of the time-of-flight calculations presented in this paper, we require a statistical survey of how the spatial distributions vary with Dst index based on spacecraft observations.

In contrast to the spatial distributions of field line eigenfrequency observed in the magnetic equatorial plane, the distribution mapped to the ionospheric footprints of the field lines exhibit differing trends. However, it is noted that a detailed comparison is restricted by the limited latitudinal ranges where the eigenfrequency profiles overlap, Figures 1, 4, and 5 show that for increasingly negative values of the Dst index the eigenfrequency of a given field line is generally reduced, and the change in eigenfrequency is up to $\sim$ 3 mHz. Considering the contribution from the magnetic field that acts to decrease the eigenfrequency and the competing mass density that acts to increase the eigenfrequency, the results demonstrate that magnetic field variations dominate over changes in the mass density, resulting in decreased frequencies for increasing ring current strength. This is not an unexpected result. Equation (1) indicates the smaller contribution of the mass density compared to the magnetic field strength in determining the Alfvén speed. Furthermore, Sandhu, Yeoman, et al. (2018) showed the dominance of the magnetic field configuration over the mass density distribution in shaping the spatial variations of eigenfrequencies. Figures 4 and 5 also show that the change in eigenfrequency with geomagnetic activity is greater for field lines at lower footprint latitudes. As the ring current strength peaks at $L \sim 4$ during quiet times and moves inward during enhanced storm times (Jorgensen et al., 2004; Sandhu, Rae, et al., 2018; Zhao et al., 2015), it is expected that the magnetic field perturbation will be greater for the

field lines at the lower footprint latitudes of the range considered in the time-of-flight calculations. Therefore, the field lines at lower footprint latitudes will have a greater sensitivity to changes in the ring current intensity, as represented by the Dst index.

In addition to the ring current related magnetic field perturbations, which act to weaken and expand the background magnetic field, the field configuration also experiences contributions from the solar wind. As shown in Table 1, during active conditions the solar wind pressure is also enhanced, which acts the compress the magnetosphere and strengthen the magnetic field. This contribution would act to increase the field line eigenfrequency. However, for the *L* range considered in this study and the range of solar wind pressures applied (Table 1), the ring current perturbation is dominant and outweighs any contribution from solar wind compression of the magnetic field.

Direct ground-based measurements of FLR frequencies support the time-of-flight calculations presented here, where decreased frequencies are observed during disturbed conditions (Du et al., 2005; Gupta, 1974; Warner & Orr, 1979). Some previous observations have been used to infer changes in the mass density distribution. Based on the observed decrease in eigenfrequency and the relation between the Alfvén speed and the mass density, previous authors have attributed the change in eigenfrequency to an increased mass density (e.g., Takahashi et al., 2002). The result was reasoned by an increased heavy ion concentration, known to occur during enhanced levels of geomagnetic activity (Maeda et al., 2009; Maggiolo & Kistler, 2014; Mouikis et al., 2010; Nosé et al., 2009; Ohtani et al., 2011; Sandhu et al., 2017; Takahashi et al., 2006; Young et al., 1982). However, subsequent work has established that due to a strong depletion of the inner magnetospheric plasma population, the mass density in this region is decreased during geomagnetically active periods (Sandhu et al., 2017). It is shown here that the decrease in eigenfrequency is solely due to magnetic field variations, which outweigh and mask the opposing contribution from the mass density. This should be expected from the definition of the perturbation speed (equation 1), which shows that the sensitivity to the magnetic field is greater than to the mass density. Therefore, the results presented in this study highlight that the magnetic field configuration is an essential factor that should be accounted for when inferring the mass density from eigenfrequencies, particularly for assessing variations with geomagnetic activity. Furthermore, the difference in profiles when mapping the magnetic equatorial plane and the ionospheric footprints of the field lines demonstrate the significant role of the magnetic field configuration in shaping the observed changes in field line eigenfrequency.

Another notable feature of the time-of-flight calculations is how the MLT location of minimum frequency values varies with Dst index, as apparent from Figures 1, 3, and 5. For quiet times, the time-of-flight frequencies approach a minimum in the evening MLT sector. This asymmetry agrees well with previous results (Junginger & Baumjohann, 1984; Liu et al., 2009; Mathie et al., 1999; Plaschke et al., 2008; Poulter et al., 1984; Sandhu, Yeoman, et al., 2018; Takahashi et al., 2015, 2016; Takahashi & McPherron, 1984; Takahashi et al., 1984; Yumoto et al., 1983), where increased field line length and decreased field magnitude for the comparatively stretched nightside field lines act to decrease the field line eigenfrequencies compared to the dayside. In addition, the mass density distribution during quiet geomagnetic conditions maximizes in the evening sector due to the shape of the plasmasphere and the enhancement of heavy ion concentration (Sandhu et al., 2017). This reduces the Alfvén speed in the evening sector (equation (1)) and results in a shift in the eigenfrequency MLT asymmetry, where the minimum eigenfrequency is located in the premidnight MLT sector (Sandhu, Yeoman, et al., 2018). For increasing Dst index, representing increasing levels of geomagnetic activity, the MLT location of the minimum eigenfrequency shifts to earlier MLT sectors, toward noon. Furthermore, Figure 3 shows significant enhancements in eigenfrequency in the dusk sector. This dependence was not present in the time-of-flight calculations of Wild et al. (2005), where only magnetic field variations were considered, and, therefore, can be attributed solely to the mass density contributions. The Sandhu et al. (2017) mass density model shows that due to the sunward rotation of the plasmaspheric bulge with increased magnetospheric convection, the MLT location of peak mass density values moves from dusk to noon. As increased mass density values correspond to decreased Alfvén speed (equation (1)), and therefore decreased time-of-flight frequencies (equation (2)), the MLT dependence of the estimated frequencies is a direct consequence of the mass density variations.

A key motivation of this study was related to understanding the storm time energization of the radiation belts through wave-particle interactions. Magnetohydrodynamic waves that are generated at the dayside magnetopause (e.g., Chen & Hasegawa, 1974; Claudepierre et al., 2009; Glassmeier et al., 1984; Russell & Elphic, 1978)

generally propagate throughout the magnetosphere in the antisunward direction (Allan & Poulter, 1992) and result in the flow of energy in the form of compressional waves (Kivelson & Southwood, 1988; Lysak & Lee, 1992). The compressional waves can couple with toroidal and poloidal FLRs in the inner magnetosphere where the local field line eigenfrequency matches the compressional wave frequency (Allan & Poulter, 1992; Elsden & Wright, 2017; 2018; Mann et al., 1995; Rae et al., 2005; Walker, 2000). Therefore, the location at which the FLRs are driven by the coupling is dependent on the spatial distribution of eigenfrequency. As previous work has established, the occurrence of FLRs are known to be an important process in the energization of electron to relativistic energies and the generation of the storm time radiation belts (Baker, Pulkkinen, Li, Kanekal, Blake, et al., 1998, Baker, Pulkkinen, Li, Kanekal, Ogilvie, et al., 1998; Blake, Gussenhoven, et al. 1992; Blake, Kolasinski, et al. 1992; Li et al., 1998; Green & Kivelson, 2001; Mathie & Mann, 2000; Nakamura et al., 2002; O'Brien & Moldwin, 2003; Reeves et al., 2003; Rostoker et al., 1998). The results shown here demonstrate a decrease in the eigenfrequency with increased levels of geomagnetic activity, which suggests that during storm times the compressional waves can couple to field lines with lower footprint latitudes values and excite higher amplitudes (Degeling et al., 2018). Furthermore, the local time asymmetry in eigenfrequency and how this asymmetry changes with ring current intensity has important implications on the polarization of the Alfvén waves as well as the characteristics of FLRs (Elsden & Wright, 2018; Kabin et al., 2007; Wright et al., 2018). The MLT asymmetries are further demonstrated in Figure S1 in the supporting information, where we reproduce Figures 1a–1d with line contours as opposed to a color contour. Figure S1 illustrates how the resonant surface of field lines forms asymmetric contours of frequency. Overall, the results presented in this study have significant implications for understanding how wave resonance structures vary with geomagnetic activity.

Although the time-of-flight calculations shown here represent improved and more realistic estimates compared to previous work, it is important to note the restrictions of the results. The approach relies on the validity of both the mass density and magnetic field models. It has been established that the T96 magnetic field model can overestimate the ring current perturbation to the geomagnetic field at times (Zhang et al., 2010), which would act to underestimate the frequencies in the time-of-flight calculations. In addition, the Sandhu et al. (2017) mass density model is based on an average of multiple measurements at different locations for a data set spanning from 2001 to 2012. Therefore, it contains a large amount of variability due to solar cycle effects and solar wind conditions that are not incorporated into the model. Regardless of these limitations, both these models provide a significantly improved characterization of the magnetic field and mass density distribution for varying levels of geomagnetic activity. Through the time-of-flight approach we have been able to provide a more realistic distribution of field line eigenfrequencies for all local times within $5.9 \leq L < 9.5$ and how they vary with geomagnetic activity. In order to further establish the validity of these estimates, future work should compare the results to a substantially large (both spatially and temporally) data set of direct FLR observations (e.g., Sandhu, Yeoman, et al., 2018; Wharton et al., 2018).

This study also highlights that in order to have a more complete and global understanding of FLRs, the plasma regimes outside of $5.9 \leq L < 9.5$ require consideration. For example, Vellante et al. (2007) show that at lower L values, well within the plasmasphere, the eigenfrequencies exhibit significantly different dependences and trends. Understanding how the magnetic field and mass density contributions combine for different plasma regimes will provide a fuller understanding of how wave energy can propagate throughout the magnetospheric system.

5. Summary and Conclusions

The time-of-flight technique has been utilized with realistic descriptions of the geomagnetic field and plasma mass density distribution to explore how field line eigenfrequencies vary with the ring current strength. We considered field lines spanning all local times within $5.9 \leq L < 9.5$, for Dst index values between −100 and 0 nT. The results indicate important dependences on the magnetic field configuration with varying geomagnetic activity and highlights the necessity to consider how the field line mapping changes with ring current intensity. By mapping observations to the ionospheric footprints, we are able to monitor changes in eigenfrequency for a given field line with increasing geomagnetic activity. The results indicated a general decrease in the field line eigenfrequencies for increasingly active conditions, which agrees well with previous direct observations of FLRs. The time-of-flight approach allowed the magnetic field and mass density contributions to be isolated, and it was found that the magnetic field contribution dominates and outweighs variations in the mass density with geomagnetic activity. This has important implications for inferring mass density changes from FLR observations, and emphasizes the need to account for magnetic field variations. Overall,

the time-of-flight estimates shown here present a simple and quick means to estimate the eigenfrequency for a field line with a defined location and level of geomagnetic activity.

The results presented in this study examine variations with the ring current strength. However, this represents only one aspect of magnetospheric variability. Other factors, such as substorms, are known to affect the eigenfrequency values through changes in the magnetic field configuration and mass density distribution. Future work could aim to assess dependences on different aspects of magnetospheric variability, and therefore provide a more valid estimation of eigenfrequencies for given conditions.

We emphasize the important applications of the eigenfrequency estimates in the inner magnetosphere for varying levels of geomagnetic activity in further understanding storm time dynamics. By establishing how the eigenfrequency varies with distance from the magnetopause allows insight into where wave energy can couple to FLRs, which can then drive energization of electrons and contribute to the storm time radiation belts. In this study we have supported the modeling results of Degeling et al. (2018) and the results suggest that wave energy can penetrate to field lines at higher invariant magnetic latitudes during storm times.

Acknowledgments
J. K. S. is supported by STFC consolidated grant ST/N0007722/1 and NERC grant NE/L007495/1. T. K. Y. is supported by STFC grant ST/H002480/1 and NERC grant NE/K011766/1. I. J. R. is supported in part by STFC consolidated grant ST/N0007722/1 and NERC grant NE/L007495/1. This study utilized data from the CARISMA ground magnetometer array, which are available from http://carisma.ca. The authors thank I. R. Mann, D. K. Milling, and the rest of the CARISMA team for data. CARISMA is operated by the University of Alberta, funded by the Canadian Space Agency.

References

Akasofu, S.-I., & Chapman, S. (1961). The ring current, geomagnetic disturbance, and the Van Allen radiation belts. *Journal of Geophysical Research*, *66*, 1321–1350. https://doi.org/10.1029/JZ066i005p01321

Akasofu, S.-I., Chapman, S., & Venkatesan, B. (1963). The main phase of great magnetic storms. *Journal of Geophysical Research*, *68*, 3345–3350. https://doi.org/10.1029/JZ068i011p03345

Allan, W., & Poulter, E. M. (1992). ULF waves—Their relationship to the structure of the Earth's magnetosphere. *Reports on Progress in Physics*, *55*, 533–598. https://doi.org/10.1088/0034-4885/55/5/001

Baker, D. N., Pulkkinen, T. I., Li, X., Kanekal, S. G., Blake, J. B., Selesnick, R. S., et al. (1998). Coronal mass ejections, magnetic clouds, and relativistic magnetospheric electron events: ISTP. *Journal of Geophysical Research*, *103*(A8), 17,279–17,291. https://doi.org/10.1029/97JA03329

Baker, D. N., Pulkkinen, T. I., Li, X., Kanekal, S. G., Ogilvie, K. W., Lepping, R. P., et al. (1998). A strong CME related magnetic cloud interaction with the Earth's magnetosphere: ISTP observations of rapid relativistic electron acceleration on May 15, 1997. *Geophysical Research Letters*, *25*(15), 2975–2978. https://doi.org/10.1029/98GL01134

Bartels, J., Heck, N. H., & Johnston, H. F. (1939). The three-hour-range index measuring geomagnetic activity. *Terrestrial Magnetism and Atmospheric Electricity*, *44*(4), 411–454. https://doi.org/10.1029/TE044i004p00411

Baumjohann, W., & Treumann, R. (1996). *Basic Space Plasma Physics* London: Imperial College Press.

Blake, J. B., Gussenhoven, M. S., Mullen, E. G., & Fillius, R. W. (1992). Identification of an unexpected space radiation hazard. *IEEE Transactions on Nuclear Science*, *39*, 1761–1764. https://doi.org/10.1109/23.211364

Blake, J. B., Kolasinski, W. A., Fillius, R. W., & Mullen, E. G. (1992). Injection of electrons and protons with energies of tens of MeV into $L < 3$ on 24 March 1991. *Geophysical Research Letters*, *19*(8), 821–824. https://doi.org/10.1029/92GL00624

Cahill, L. J. (1966). Inflation of the inner magnetosphere during a magnetic storm. *Journal of Geophysical Research*, *71*(19), 4505–4519. https://doi.org/10.1029/JZ071i019p04505

Cahill, L. J. (1970). Magnetosphere inflation during four magnetic storms in 1965. *Journal of Geophysical Research*, *75*(19), 3778–3788. https://doi.org/10.1029/JA075i019p03778

Chapman, S. (1918). An outline of a theory of magnetic storms. *Royal Society of London Proceedings Series A*, *95*, 61–83. https://doi.org/10.1098/rspa.1918.0049

Chapman, S., & Bartels, J. (1940). *Geomagnetism, no. v. 1 in The International Series of Monographs on Physics*. Oxford: Clarendon Press.

Chappell, C. R. (1972). Recent satellite measurements of the morphology and dynamics of the plasmasphere. *Reviews of Geophysics*, *10*, 951–979. https://doi.org/10.1029/RG010i004p00951

Chen, L., & Hasegawa, A. (1974). A theory of long-period magnetic pulsations: 1. Steady state excitation of field line resonance. *Journal of Geophysical Research*, *79*(7), 1024–1032. https://doi.org/10.1029/JA079i007p01024

Claudepierre, S. G., Wiltberger, M., Elkington, S. R., Lotko, W., & Hudson, M. K. (2009). Magnetospheric cavity modes driven by solar wind dynamic pressure fluctuations. *Geophysical Research Letters*, *36*, L13101. https://doi.org/10.1029/2009GL039045

Degeling, A. W., Rae, I. J., Watt, C. E. J., Shi, Q. Q., Rankin, R., & Zong, Q. (2018). Control of ULF wave accessibility to the inner magnetosphere by the convection of plasma density. *Journal of Geophysical Research: Space Physics*, *123*, 1086–1099. https://doi.org/10.1002/2017JA024874

Dessler, A. J., & Parker, E. N. (1959). Hydromagnetic theory of geomagnetic storms. *Journal of Geophysical Research*, *64*, 2239–2252. https://doi.org/10.1029/JZ064i012p02239

Du, A., Sun, W., Xu, W., & Gao, X. (2005). The frequency variation of Pc5 ULF waves during a magnetic storm, Earth. *Planets and Space*, *57*(7), 619–625. https://doi.org/10.1186/BF03351841

Dungey, J. W. (1954a). Electrodynamics of the outer atmosphere. *Pennsylvania State University Ionosphere Research Laboratory Science Report*, *69*, 51.

Dungey, J. W. (1954b). The propagation of Alfvén waves through the ionosphere. *Pennsylvania State University Ionosphere Research Laboratory Science Report*, *57*.

Dungey, J. W. (1961). Interplanetary magnetic field and the auroral zones. *Physical Review Letters*, *6*, 47–48. https://doi.org/10.1103/PhysRevLett.6.47

Elkington, S. R., Hudson, M. K., & Chan, A. A. (1999). Acceleration of relativistic electrons via drift-resonant interaction with toroidal-mode Pc-5 ULF oscillations. *Geophysical Research Letters*, *26*, 3273–3276. https://doi.org/10.1029/1999GL003659

Elsden, T., & Wright, A. N. (2017). The theoretical foundation of 3-D Alfvén resonances: Time-dependent solutions. *Journal of Geophysical Research: Space Physics*, *122*, 3247–3261. https://doi.org/10.1002/2016JA023811

Elsden, T., & Wright, A. N. (2018). The broadband excitation of 3-D Alfvén resonances in a MHD waveguide. *Journal of Geophysical Research: Space Physics*, *123*, 530–547. https://doi.org/10.1002/2017JA025018

Engebretson, M. J., & Cahill, L. J. (1981). Pc5 pulsations observed during the June 1972 geomagnetic storm. *Journal of Geophysical Research*, *86*, 5619–5631. https://doi.org/10.1029/JA086iA07p05619
Engebretson, M. J., Zanetti, L. J., Potemra, T. A., & Acuna, M. H. (1986). Harmonically structured ULF pulsations observed by the AMPTE CCE magnetic field experiment. *Geophysical Research Letters*, *13*, 905–908. https://doi.org/10.1029/GL013i009p00905
Ganushkina, N. Y., Liemohn, M. W., Kubyshkina, M. V., Ilie, R., & Singer, H. J. (2010). Distortions of the magnetic field by storm-time current systems in Earth's magnetosphere. *Annales Geophysicae*, *28*, 123–140. https://doi.org/10.5194/angeo-28-123-2010
Glassmeier, K. H., Volpers, H., & Baumjohann, W. (1984). Ionospheric Joule dissipation as a damping mechanism for high latitude ULF pulsations—Observational evidence. *Planetary and Space Science*, *32*, 1463–1466. https://doi.org/10.1016/0032-0633(84)90088-6
Goertz, C. K., & Smith, R. A. (1989). The thermal catastrophe model of substorms. *Journal of Geophysical Research*, *94*(A6), 6581–6596. https://doi.org/10.1029/JA094iA06p06581
Gonzalez, W. D., Joselyn, J. A., Kamide, Y., Kroehl, H. W., Rostoker, G., Tsurutani, B. T., & Vasyliunas, V. M. (1994). What is a geomagnetic storm. *Journal of Geophysical Research*, *99*, 5771–5792. https://doi.org/10.1029/93JA02867
Green, J. C., & Kivelson, M. G. (2001). A tale of two theories: How the adiabatic response and ULF waves affect relativistic electrons. *Journal of Geophysical Research*, *106*(A11), 25,777–25,791. https://doi.org/10.1029/2001JA000054
Gupta, J. C. (1974). Amplitude variation of Pc 5 pulsations at high latitudes. *Radio Science*, *9*(8-9), 757–768. https://doi.org/10.1029/RS009i008p00757
Hartinger, M., Angelopoulos, V., Moldwin, M. B., Glassmeier, K.-H., & Nishimura, Y. (2011). Global energy transfer during a magnetospheric field line resonance. *Geophysical Research Letters*, *38*, L12101. https://doi.org/10.1029/2011GL047846
Iyemori, T. (1990). Storm-time magnetospheric currents inferred from mid-latitude geomagnetic field variations. *Journal of Geomagnetism and Geoelectricity*, *42*, 1249–1265.
Jorgensen, A. M., Spence, H. E., Hughes, W. J., & Singer, H. J. (2004). A statistical study of the global structure of the ring current. *Journal of Geophysical Research*, *109*, A12204. https://doi.org/10.1029/2003JA010090
Junginger, H., & Baumjohann, W. (1984). Resonant harmonic Alfvén waves in the magnetosphere—A case study. *Journal of Geophysical Research*, *89*, 10,757–10,762. https://doi.org/10.1029/JA089iA12p10757
Kabin, K., Rankin, R., Mann, I. R., Degeling, A. W., & Marchand, R. (2007). Polarization properties of standing shear Alfvén waves in non-axisymmetric background magnetic fields. *Annales Geophysicae*, *25*(3), 815–822. https://doi.org/10.5194/angeo-25-815-2007
Kivelson, M. G., & Southwood, D. J. (1988). Hydromagnetic waves and the ionosphere. *Geophysical Research Letters*, *15*(11), 1271–1274. https://doi.org/10.1029/GL015i011p01271
Lee, D. H., & Lysak, R. L. (1990). Effects of azimuthal asymmetry on ULF waves in the dipole magnetosphere. *Geophysical Research Letters*, *17*(1), 53–56. https://doi.org/10.1029/GL017i001p00053
Li, X., Baker, D. N., Temerin, M., Cayton, T., Reeves, G. D., Araki, T., et al. (1998). Energetic electron injections into the inner magnetosphere during the Jan. 10-11, 1997 magnetic storm. *Geophysical Research Letters*, *25*(14), 2561–2564. https://doi.org/10.1029/98GL00036
Liu, W., Sarris, T. E., Li, X., Elkington, S. R., Ergun, R., Angelopoulos, V., et al. (2009). Electric and magnetic field observations of Pc4 and Pc5 pulsations in the inner magnetosphere: A statistical study. *Journal of Geophysical Research*, *114*, A12206. https://doi.org/10.1029/2009JA014243
Lysak, R. L., & Lee, D. (1992). Response of the dipole magnetosphere to pressure pulses. *Geophysical Research Letters*, *19*(9), 937–940. https://doi.org/10.1029/92GL00625
Maeda, N., Takasaki, S., Kawano, H., Ohtani, S., Decreau, P., Trotignon, J., et al. (2009). Simultaneous observations of the plasma density on the same field line by the CPMN ground magnetometers and the Cluster satellites. *Advances in Space Research*, *43*, 265–272. https://doi.org/10.1016/j.asr.2008.04.016
Maggiolo, R., & Kistler, L. M. (2014). Spatial variation in the plasma sheet composition: Dependence on geomagnetic and solar activity. *Journal of Geophysical Research: Space Physics*, *119*, 2836–2857. https://doi.org/10.1002/2013JA019517
Mann, I. R., Milling, D. K., Rae, I. J., Ozeke, L. G., Kale, A., Kale, Z. C., et al. (2008). The upgraded CARISMA magnetometer array in the THEMIS era. *Space Science Reviews*, *141*, 413–451. https://doi.org/10.1007/s11214-008-9457-6
Mann, I. R., Wright, A. N., & Cally, P. S. (1995). Coupling of magnetospheric cavity modes to field line resonances: A study of resonance widths. *Journal of Geophysical Research*, *100*(A10), 19,441–19,456. https://doi.org/10.1029/95JA00820
Mathie, R. A., & Mann, I. R. (2000). A correlation between extended intervals of ULF wave power and storm-time geosynchronous relativistic electron flux enhancements. *Geophysical Research Letters*, *27*(20), 3261–3264. https://doi.org/10.1029/2000GL003822
Mathie, R. A., Menk, F. W., Mann, I. R., & Orr, D. (1999). Discrete field line resonances and the Alfvén continuum in the outer magnetosphere. *Geophysical Research Letters*, *26*, 659–662. https://doi.org/10.1029/1999GL900104
Mouikis, C. G., Kistler, L. M., Liu, Y. H., Klecker, B., Korth, A., & Dandouras, I. (2010). H^+ and O^+ content of the plasma sheet at 15-19 Re as a function of geomagnetic and solar activity. *J. Geophys. Res.*, *115*, A00J16. https://doi.org/10.1029/2010JA015978
Nakamura, R., Blake, J., Elkington, S., Baker, D., Baumjohann, W., & Klecker, B. (2002). Relationship between ULF waves and radiation belt electrons during the March 10, 1998, storm. *Advances in Space Research*, *30*(10), 2163–2168. https://doi.org/10.1016/S0273-1177(02)80210-1
Nosé, M., Ieda, A., & Christon, S. P. (2009). Geotail observations of plasma sheet ion composition over 16 years: On variations of average plasma ion mass and O^+ triggering substorm model. *Journal of Geophysical Research*, *114*, A07223. https://doi.org/10.1029/2009JA014203
O'Brien, T. P., & Moldwin, M. B. (2003). Empirical plasmapause models from magnetic indices. *Geophysical Research Letters*, *30*(4), 1152. https://doi.org/10.1029/2002GL016007
Obayashi, T., & Jacobs, J. A. (1958). Geomagnetic pulsations and the Earth's outer atmosphere. *Geophysical Journal*, *1*, 53–63. https://doi.org/10.1111/j.1365-246X.1958.tb00034.x
Ohtani, S., Nosé, M., Christon, S. P., & Lui, A. T. Y. (2011). Energetic O^+ and H^+ ions in the plasma sheet: Implications for the transport of ionospheric ions. *Journal of Geophysical Research*, *116*, A10211. https://doi.org/10.1029/2011JA016532
Orr, D., & Matthew, J. A. D. (1971). The variation of geomagnetic micropulsation periods with latitude and the plasmapause. *Planetary and Space Science*, *19*, 897–905. https://doi.org/10.1016/0032-0633(71)90141-3
Parker, E. N., & Stewart, H. A. (1967). Nonlinear inflation of a magnetic dipole. *Journal of Geophysical Research*, *72*, 5287–5293. https://doi.org/10.1029/JZ072i021p05287
Plaschke, F., Glassmeier, K.-H., Constantinescu, O. D., Mann, I. R., Milling, D. K., Motschmann, U., & Rae, I. J. (2008). Statistical analysis of ground based magnetic field measurements with the field line resonance detector. *Annales Geophysicae*, *26*, 3477–3489. https://doi.org/10.5194/angeo-26-3477-2008
Poulter, E. M., Allan, W., Keys, J. G., & Nielsen, E. (1984). Plasmatrough ion mass densities determined from ULF pulsation eigenperiods. *Planetary and Space Science*, *32*, 1069–1078. https://doi.org/10.1016/0032-0633(84)90132-6

Rae, I. J., Donovan, E. F., Mann, I. R., Fenrich, F. R., Watt, C. E. J., Milling, D. K., et al. (2005). Evolution and characteristics of global Pc5 ULF waves during a high solar wind speed interval. *Journal of Geophysical Research*, *110*, A12211. https://doi.org/10.1029/2005JA011007

Rae, I. J., Watt, C. E. J., Fenrich, F. R., Mann, I. R., Ozeke, L. G., & Kale, A. (2007). Energy deposition in the ionosphere through a global field line resonance. *Annales Geophysicae*, *25*(12), 2529–2539. https://doi.org/10.5194/angeo-25-2529-2007

Reeves, G. D., McAdams, K. L., Friedel, R. H. W., & O'Brien, T. P. (2003). Acceleration and loss of relativistic electrons during geomagnetic storms. *Geophysical Research Letters*, *30*(10), 1529. https://doi.org/10.1029/2002GL016513

Rostoker, G., Skone, S., & Baker, D. N. (1998). On the origin of relativistic electrons in the magnetosphere associated with some geomagnetic storms. *Geophysical Research Letters*, *25*(19), 3701–3704. https://doi.org/10.1029/98GL02801

Russell, C. T., & Elphic, R. C. (1978). Initial ISEE magnetometer results: Magnetopause observations. *Space Science Reviews*, *22*(6), 681–715. https://doi.org/10.1007/BF00212619

Samson, J. C., Jacobs, J. A., & Rostoker, G. (1971). Latitude-dependent characteristics of long-period geomagnetic micropulsations. *Journal of Geophysical Research*, *76*, 3675–3683. https://doi.org/10.1029/JA076i016p03675

Samson, J. C., & Rostoker, G. (1972). Latitude-dependent characteristics of high-latitude Pc 4 and Pc 5 micropulsations. *Journal of Geophysical Research*, *77*, 6133–6144. https://doi.org/10.1029/JA077i031p06133

Sandhu, J. K., Rae, I. J., Freeman, M. P., Forsyth, C., Gkioulidou, M., Reeves, G. D., et al. (2018). Energization of the ring current by substorms. *Journal of Geophysical Research: Space Physics*, *123*. https://doi.org/10.1029/2018JA025766

Sandhu, J. K., Yeoman, T. K., Fear, R. C., & Dandouras, I. (2016a). A statistical study of magnetospheric ion composition along the geomagnetic field using the Cluster spacecraft for L values between 5.9 and 9.5. *Journal of Geophysical Research: Space Physics*, *121*, 2194–2208. https://doi.org/10.1002/2015JA022261

Sandhu, J. K., Yeoman, T. K., Fear, R. C., & Dandouras, I. (2016b). A statistical study of magnetospheric electron density using the Cluster spacecraft. *Journal of Geophysical Research: Space Physics*, *121*, 11,042–11,062. https://doi.org/10.1002/2016JA023397

Sandhu, J. K., Yeoman, T. K., James, M. K., Rae, I. J., & Fear, R. C. (2018). Variations of high-latitude geomagnetic pulsation frequencies: A comparison of time-of-flight estimates and IMAGE magnetometer observations. *Journal of Geophysical Research: Space Physics*, *123*, 567–586. https://doi.org/10.1002/2017JA024434

Sandhu, J. K., Yeoman, T. K., Rae, I. J., Fear, R. C., & Dandouras, I. (2017). The dependence of magnetospheric plasma mass loading on geomagnetic activity using Cluster. *Journal of Geophysical Research: Space Physics*, *122*, 9371–9395. https://doi.org/10.1002/2017JA024171

Sckopke, N. (1966). A general relation between the energy of trapped particles and the disturbance field near the Earth. *Journal of Geophysical Research*, *71*, 3125–3130. https://doi.org/10.1029/JZ071i013p03125

Singer, H. J., Southwood, D. J., Walker, R. J., & Kivelson, M. G. (1981). Alfven wave resonances in a realistic magnetospheric magnetic field geometry. *Journal of Geophysical Research*, *86*, 4589–4596. https://doi.org/10.1029/JA086iA06p04589

Snyder, C. W., Neugebauer, M., & Rao, U. R. (1963). The solar wind velocity and its correlation with cosmic-ray variations and with solar and geomagnetic activity. *Journal of Geophysical Research*, *68*(24), 6361–6370. https://doi.org/10.1029/JZ068i024p06361

Southwood, D. J. (1974). Some features of field line resonances in the magnetosphere. *Planetary and Space Science*, *22*, 483–491. https://doi.org/10.1016/0032-0633(74)90078-6

Sugiura, M., & Kamei, T. (1991). Equatorial Dst index 1957–1986. In A. Berthelier & M. Menvielle (Eds.), *IAGA Bull.* (Vol. 40, pp. 6–14). France: ISGI Publ. Off., Saint. Maur-des-Fosses.

Sugiura, M., & Poros, D. J. (1964). Hourly values of equatorial Dst for the IGY. *Annals of the International Geophysical Year*, *35*, 9–45.

Takahashi, K., Denton, R. E., Anderson, R. R., & Hughes, W. J. (2004). Frequencies of standing Alfvén wave harmonics and their implication for plasma mass distribution along geomagnetic field lines: Statistical analysis of CRRES data. *Journal of Geophysical Research*, *109*, A08202. https://doi.org/10.1029/2003JA010345

Takahashi, K., Denton, R. E., Anderson, R. R., & Hughes, W. J. (2006). Mass density inferred from toroidal wave frequencies and its comparison to electron density. *Journal of Geophysical Research*, *111*, A01201. https://doi.org/10.1029/2005JA011286

Takahashi, K., Denton, R. E., & Gallagher, D. (2002). Toroidal wave frequency at L = 6–10: Active Magnetospheric Particle Tracer Explorers/CCE observations and comparison with theoretical model. *Journal of Geophysical Research*, *107*, 1020. https://doi.org/10.1029/2001JA000197

Takahashi, K., Hartinger, M. D., Angelopoulos, V., & Glassmeier, K.-H. (2015). A statistical study of fundamental toroidal mode standing Alfvén waves using THEMIS ion bulk velocity data. *Journal of Geophysical Research: Space Physics*, *120*, 6474–6495. https://doi.org/10.1002/2015JA021207

Takahashi, K., Lee, D.-H., Merkin, V. G., Lyon, J. G., & Hartinger, M. D. (2016). On the origin of the dawn-dusk asymmetry of toroidal Pc5 waves. *Journal of Geophysical Research: Space Physics*, *121*, 9632–9650. https://doi.org/10.1002/2016JA023009

Takahashi, K., & McPherron, R. L. (1984). Standing hydromagnetic oscillations in the magnetosphere. *Planetary and Space Science*, *32*, 1343–1359.

Takahashi, K., McPherron, R. L., & Hughes, W. J. (1984). Multispacecraft observations of the harmonic structure of Pc 3–4 magnetic pulsations. *Journal of Geophysical Research*, *89*, 6758–6774. https://doi.org/10.1029/JA089iA08p06758

Thomsen, M. F. (2004). Why Kp is such a good measure of magnetospheric convection. *Space Weather*, *2*, S11004. https://doi.org/10.1029/2004SW000089

Tsyganenko, N. A. (1995). Modeling the Earth's magnetospheric magnetic field confined within a realistic magnetopause. *Journal of Geophysical Research*, *100*(A4), 5599–5612. https://doi.org/10.1029/94JA03193

Tsyganenko, N. A. (1996). B Effects of the solar wind conditions in the global magnetospheric configurations as deduced from data-based field models (Invited). In E. J. Rolfe (Ed.), *International conference on substorms* (Vol. 389, pp. 181). Kaldeich: ESA Special Publication.

Tsyganenko, N. A., & Mukai, T. (2003). Tail plasma sheet models derived from Geotail particle data. *Journal of Geophysical Research*, *108*(A3), 1136. https://doi.org/10.1029/2002JA009707

Vellante, M., FÄürster, M., Villante, U., Zhang, T. L., & Magnes, W. (2007). Solar activity dependence of geomagnetic field line resonance frequencies at low latitudes. *Journal of Geophysical Research*, *112*, A02205. https://doi.org/10.1029/2006JA011909

Walker, A (2000). Coupling between waveguide modes and field line resonances. *Journal of Atmospheric and Solar-Terrestrial Physics*, *62*(9), 799–813. https://doi.org/10.1016/S1364-6826(00)00046-8

Warner, M. R., & Orr, D. (1979). Time of flight calculations for high latitude geomagnetic pulsations. *Planetary and Space Science*, *27*, 679–689. https://doi.org/10.1016/0032-0633(79)90165-X

Waters, C. L., Menk, F. W., & Fraser, B. J. (1991). The resonance structure of low latitude Pc3 geomagnetic pulsations. *Geophysical Research Letters*, *18*, 2293–2296. https://doi.org/10.1029/91GL02550

Wharton, S. J., Wright, D. M., Yeoman, T. K., James, M. K., & Sandhu, J. K. (2018). Cross-phase determination of ultralow frequency wave harmonic frequencies and their associated plasma mass density distributions. *Journal of Geophysical Research: Space Physics*, *123*, 6231–6250. https://doi.org/10.1029/2018JA025487

Wilcox, J. M., Schatten, K. H., & Ness, N. F. (1967). Influence of interplanetary magnetic field and plasma on geomagnetic activity during quiet-Sun conditions. *Journal of Geophysical Research*, *72*(1), 19–26. https://doi.org/10.1029/JZ072i001p00019

Wild, J. A., Yeoman, T. K., & Waters, C. L. (2005). Revised time-of-flight calculations for high-latitude geomagnetic pulsations using a realistic magnetospheric magnetic field model. *Journal of Geophysical Research*, *110*, A11206. https://doi.org/10.1029/2004JA010964

Wright, A. N., Elsden, T., & Takahashi, K. (2018). Modeling the dawn/dusk asymmetry of field line resonances. *Journal of Geophysical Research: Space Physics*, *123*, 6443–6456. https://doi.org/10.1029/2018JA025638

Young, D. T., Balsiger, H., & Geiss, J. (1982). Correlations of magnetospheric ion composition with geomagnetic and solar activity. *Journal of Geophysical Research*, *87*(A11), 9077–9096. https://doi.org/10.1029/JA087iA11p09077

Yumoto, K., Saito, T., & Sakurai, T. (1983). Local time asymmetry in the characteristics of Pc5 magnetic pulsations. *Planetary and Space Science*, *31*, 459–471. https://doi.org/10.1016/0032-0633(83)90158-7

Zhang, Q.-H., Dunlop, M. W., Holme, R., & Woodfield, E. E. (2010). Comparison of eight years magnetic field data from Cluster with Tsyganenko models in the inner magnetosphere. *Annales Geophysicae*, *28*(1), 309–326. https://doi.org/10.5194/angeo-28-309-2010

Zhang, J., Liemohn, M. W., Kozyra, J. U., Thomsen, M. F., Elliott, H. A., & Weygand, J. M. (2006). A statistical comparison of solar wind sources of moderate and intense geomagnetic storms at solar minimum and maximum. *Journal of Geophysical Research*, *111*, A01104. https://doi.org/10.1029/2005JA011065

Zhao, H., Li, X., Baker, D. N., Fennell, J. F., Blake, J. B., Larsen, B. A., et al. (2015). The evolution of ring current ion energy density and energy content during geomagnetic storms based on Van Allen Probes measurements. *Journal of Geophysical Research: Space Physics*, *120*, 7493–7511. https://doi.org/10.1002/2015JA021533